

# Cell-by-Cell Modelling of Electrical Signaling in Myelinated Axons

Alessandro Gatti<sup>[0009-0005-8275-0888]</sup>, Pietro Benedusi<sup>[0000-0001-7799-5999]</sup>, and Simone Pezzuto<sup>[0000-0002-7432-0424]</sup>

## 1 Introduction

The EMI model [22], also known as cell-by-cell model, is based on three essential components in electrophysiology: the extracellular space (E), the cell membrane (M), and the intracellular space (I). In this framework, subdomains boundaries (i.e., biological membranes) are encoded explicitly, enabling physiological simulations in heterogeneous environments and resolving complex cellular-scale geometries. In contrast, traditional PDE-based physiological models, such as mono- and bidomain models, are homogeneous and are not viable at the cellular scale.

The EMI model has been previously used to study neurons [21] and cardiac tissue [20]. In our work, we simulate electrical conduction on myelinated axons, to an unprecedented level of detail, in three dimensions. In fact, previous computational work in this context considers some degree of idealization in the geometrical setting (such as considering a small portion of axon and/or a 2D geometry) [7, 9, 17, 18, 19]. In particular, we analyze two biological scenarios in which spatial and temporal dynamics are necessary to accurately model the propagation and induction of action potentials. Specifically, we investigate the effects of myelination and ephaptic coupling in axon bundles. Studying ephaptic coupling, or signaling through extracellular spaces, can improve our understanding of network-level feedback under healthy and pathological conditions.

---

Alessandro Gatti  
Simula Research Laboratory, Oslo, Norway, e-mail: [alessandro@simula.no](mailto:alessandro@simula.no)

Pietro Benedusi  
Università della Svizzera Italiana, Lugano, Switzerland, e-mail: [benedp@usi.ch](mailto:benedp@usi.ch)

Simone Pezzuto  
Università degli Studi di Trento, Trento, Italy, e-mail: [simone.pezzuto@unitn.it](mailto:simone.pezzuto@unitn.it)

## 2 The EMI model

The EMI model describes the evolution of electrical potential in cellular geometries. It consists of a system of PDEs in the bulk and a system of ODEs on the cellular membrane. The domain is  $\Omega = \Omega_i \cup \Omega_e \cup \Gamma \subset \mathbb{R}^3$ , where  $\Omega_i$  and  $\Omega_e$  are the intra- and extra-cellular domains, respectively, and  $\Gamma = \partial\Omega_i/\partial\Omega$  is the cellular membrane. For each physical region  $\Omega_r$ , with  $r \in \{i, e\}$ , we model the electrical potential  $\phi_r : \overline{\Omega_r} \times [0, T] \rightarrow \mathbb{R}$ , for  $t \in (0, T]$ :

$$-\nabla \cdot (\sigma_r \nabla \phi_r(\mathbf{x}, t)) = 0, \quad \text{for } \mathbf{x} \in \Omega_r, \quad (1)$$

$$\sigma_e \nabla \phi_e(\mathbf{x}, t) \cdot \mathbf{n}_e = -\sigma_i \nabla \phi_i(\mathbf{x}, t) \cdot \mathbf{n}_i \equiv I_M(\mathbf{x}, t), \quad \text{for } \mathbf{x} \in \Gamma, \quad (2)$$

where  $\sigma_e, \sigma_i \in \mathbb{R}_+$  are conductivities and  $\mathbf{n}_i$  (resp.  $\mathbf{n}_e$ ) is the outer normal on  $\partial\Omega_i$  (resp.  $\partial\Omega_e$ ). Note that  $\mathbf{n}_e = -\mathbf{n}_i$ . The membrane current  $I_M : \Gamma \times [0, T] \rightarrow \mathbb{R}$  can be written as the sum of two contributions, a capacitive and a ionic current:

$$I_M = I_{\text{cap}} + I_{\text{ion}} = C_M \frac{\partial \phi_M}{\partial t} + \sum_{k \in K} I_{\text{ion},k}, \quad (3)$$

where the membrane potential  $\phi_M = \phi_i - \phi_e$  stems from the capacitor-voltage equation, given a capacitance  $C_M \in \mathbb{R}_+$ . For the ionic currents  $I_{\text{ion},k}$ , describing membrane dynamics of axons, we consider the Hodgkin-Huxley equations [14] for the set of ions  $K = \{\text{Na}^+, \text{K}^+\}$ , as in [17, 8, 10, 24, 13, 18, 7, 23]. In particular,  $I_{\text{ion},k} = g_{\text{tot},k}(\phi_M - E_k)$ , where  $g_{\text{tot},k}$  collects all contributions to conductivity for ion  $k \in K$ , and  $E_k \in \mathbb{R}$  is the ion-specific reversal potential. The total ionic current is then given by

$$I_{\text{ion}} = \sum_{k \in K} I_{\text{ion},k} = g_{\text{tot}} \phi_M - E_{\text{tot}}, \quad (4)$$

where  $g_{\text{tot}} = \sum_{k \in K} g_{\text{tot},k}$  and  $E_{\text{tot}} = \sum_{k \in K} g_{\text{tot},k} E_k$ . Equations (1) represents of two Poisson problems coupled at the interface  $\Gamma$  via a time-dependent Robin condition in (2)-(3). We close the system by imposing an initial membrane potential  $\phi_M^{\text{in}} \in L^2(\Gamma)$ :

$$\phi_M(\mathbf{x}, 0) = \phi_M^{\text{in}}(\mathbf{x}), \quad \text{for } \mathbf{x} \in \Gamma,$$

and homogeneous Neumann boundary conditions for  $r \in \{i, e\}$ :

$$\nabla \phi_r(\mathbf{x}, t) \cdot \mathbf{n}_r = 0, \quad \text{for } \mathbf{x} \in \partial\Omega. \quad (5)$$

Note that given the elliptic-parabolic nature of the system (1)-(2), we cannot set an initial condition for  $\phi_r$  in  $\Omega_r$ ,  $r \in \{i, e\}$ . Furthermore, the solution is defined up to a constant, thus the system is singular.

The EMI model is the combination of a system of PDEs and ODEs, corresponding to domains of different dimensionality (3D and 2D, respectively). In this sense, it can be regarded as a *multi-dimensional* or *mixed-dimensional* model. Combining multiple submodels into a global model, enforcing consistent interface conditions,

has been the central focus of domain decomposition (DD) research in recent decades. In the context of EMI, the DD is physiologically motivated, yet the resulting algebraic structures resemble those arising from DD preconditioners.

### 3 Numerical strategy

We consider a *single-dimensional* weak formulation [22], using the current-voltage relation (3) to eliminate the membrane current  $I_M$ . The weak forms are then discretized in time with first order finite difference and in space via linear Lagrangian finite elements.

#### 3.1 Variational formulation

Assuming the solution  $\phi_r$ , for  $r \in \{i, e\}$ , to be sufficiently regular over  $\Omega_r$ , we multiply the PDEs in (1) by test functions  $v_r \in V_r$ , where  $V_r(\Omega_r)$  is a sufficiently regular Hilbert space whose elements satisfy the boundary conditions in (5). In practice, the standard choice is  $H^1(\Omega_r)$ . After integrating over  $\Omega_r$  and applying integration by parts, using interface fluxes definitions (2) and boundary conditions (5), the weak EMI problem reads (with ' $\pm_i = +$ ' and ' $\pm_e = -$ '):

$$\sigma_r \int_{\Omega_r} \nabla \phi_r \cdot \nabla v_r \, dx \pm_r \int_{\Gamma} I_M v_r \, ds = 0.$$

Eliminating the membrane current  $I_M$  via the current-voltage relation (3), we obtain:

$$\sigma_r \int_{\Omega_r} \nabla \phi_r \cdot \nabla v_r \, dx + C_M \int_{\Gamma} \partial_t \llbracket \phi_r \rrbracket v_r \, ds \pm_r \int_{\Gamma} I_{\text{ion}} v_r \, ds = 0,$$

with the jump  $\llbracket \phi_r \rrbracket = \pm_r \phi_M = \phi_r - \phi_{r'}$  for  $r' = \{i, e\}/r$ . We refer to [12] and [22, Section 6.2.1] for boundedness and coercivity results for this formulation. Making the ionic current  $I_{\text{ion}}$  explicit, according to (4), we obtain the following variational problem: for  $r \in \{i, e\}$  find  $\phi_r \in V_r$  such that

$$\sigma_r \int_{\Omega_r} \nabla \phi_r \cdot \nabla v_r \, dx + \int_{\Gamma} (C_M \partial_t + g_{\text{tot}}) \llbracket \phi_r \rrbracket v_r \, ds = \pm_r \int_{\Gamma} E_{\text{tot}} v_r \, ds, \quad (6)$$

is satisfied for all test functions  $v_r \in V_r$ .

### 3.2 Time discretization

We partition the time interval  $[0, T]$  uniformly into  $N_t$  subintervals:

$$t_n = n\Delta t, \quad \text{with } n = 0, \dots, N_t, \quad \Delta t = T/N_t,$$

and define time-discrete solution as  $\phi_r^{(n)} := \phi_r(\mathbf{x}, t_n)$  for  $\mathbf{x} \in \Omega_r$ . For the membrane dynamics, given the initial potential  $\phi_r^{(n-1)}$  at the previous time step (for  $n > 0$ ), we first solve numerically the gating variables ODEs in the Hodgkin-Huxley model using the Rush-Larsen method. This is performed with  $N_{\text{ODE}}$  steps and a step size of  $\Delta t/25$ . The updated gating variables are then used to compute  $g_{\text{tot}}^{(n)}$  and  $E_{\text{tot}}^{(n)}$ . Next, we apply implicit Euler to (6), and obtain the following semi-discrete variational problem: for  $n = 1, \dots, N_t$ , given  $\phi_r^{(n-1)}$ ,  $g_{\text{tot}}^{(n)}$ , and  $E_{\text{tot}}^{(n)}$ , find  $\phi_r^{(n)} \in V_r$  satisfying:

$$\begin{aligned} \sigma_r \int_{\Omega_r} \nabla \phi_r^{(n)} \cdot \nabla v_r \, d\mathbf{x} + \int_{\Gamma} \left( \frac{C_M}{\Delta t} + g_{\text{tot}}^{(n)} \right) \llbracket \phi_r^{(n)} \rrbracket v_r \, ds = \\ \frac{C_M}{\Delta t} \int_{\Gamma} \llbracket \phi_r^{(n-1)} \rrbracket v_r \, ds \pm_r \int_{\Gamma} E_{\text{tot}}^{(n)} v_r \, ds, \end{aligned} \quad (7)$$

for all test functions  $v_r \in V_r$ .

### 3.3 Space discretization

We discretize  $\Omega_i$  and  $\Omega_e$  by conforming tetrahedral meshes  $\mathcal{T}_i$  and  $\mathcal{T}_e$  matching on  $\Gamma$ . The Hilbert space  $V_r$  is approximated by the finite element space  $V_{r,h}$  of continuous, piecewise linear Lagrangian basis functions. For a more general description and derivation of the resulting algebraic structures and their spectral properties, we refer to [6] and to [4] for many-cell systems. We remark that the resulting EMI linear system is symmetric positive definite. The overall geometrical setting and mesh are illustrated in Figure 1 for a single myelinated axon. The membrane  $\Gamma$  is located only at the Ranvier nodes. Myelin, where the conductivity is negligible (i.e.,  $\sigma_{\text{mye}} \approx 0$ ), is not resolved by any mesh, with an advantage in terms of computational efficiency.

### 3.4 Solution strategy and implementation

The implementation<sup>1</sup> is based on the well-established FEniCS finite element software [2], using the multiphenics library<sup>2</sup> to handle variational problems coupled across multiple subdomains. The implementation is flexible in terms of ionic models

<sup>1</sup> <https://github.com/pietrobe/EMIX>

<sup>2</sup> <https://github.com/multiphenics/multiphenics>

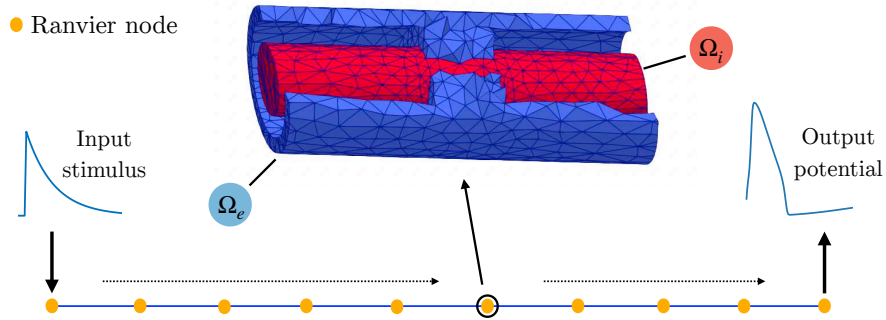


Fig. 1: Single axon geometry, showing a section of a Ranvier node mesh, where intra- and extracellular spaces are in contact. A triggering stimulus is applied at  $t = 0$  at the leftmost part and an output one is recorded at the right end. Myelin sheaths are simply treated as holes in the domain, enforcing boundary conditions in (5).

of arbitrary complexity. For meshing we used the fTetWild library [15]. As linear algebra backend, FEniCS uses PETSc. Using a fast and scalable solution strategy is crucial to handle realistic 3D setting. To this end, we use a single iteration of monolithic algebraic multigrid to precondition the conjugate gradient method. For the details of this solution strategy, we refer to [6, 5], or [16] for a recent proposal. As stopping criterion, we set a tolerance of  $10^{-6}$  for the preconditioned relative residual.

## 4 Numerical experiments

We simulate spreading potentials in two bundles of nine unmyelinated and myelinated axons arranged on a  $3 \times 3$  grid, as shown in Figure 2a, considering 10 Ranvier nodes. Table 1 presents the geometric parameters used in the simulations. For the membrane model parameters, we refer to [14]. In the myelinated case, we multiplied conductivity  $g_{\text{tot}}$  by 10, since the ionic channels are concentrated only on the Ranvier nodes [7]. The eight axons on the boundary of the myelinated and unmyelinated axon bundles are stimulated only in the first section of length  $l_{\text{node}}$ , while the axon in the middle of the bundle was not externally stimulated. Changes in membrane voltage in the central axon are observed to determine evidence of ephaptic coupling [1]. Figure 2b shows how ephaptic coupling takes place when an action potential is induced in the central axon in the unmyelinated case. There is a noticeable delay between the spike in the peripheral and central axons. Figure 2c shows that ephaptic coupling also occurs in the myelinated case, but with a very small time delay. The contrast between the induced action potentials in each case is highlighted in Figure 2d, which shows the unmyelinated and myelinated central axons side by side. We observe that although all peripheral axons were initially stimulated in the same way, the transmission of action potentials along them was not uniform. Interestingly, there is a slight delay

	Symbol	Value	Unit
intracellular conductivity	$\sigma_i$	2.01	S/m
extracellular conductivity	$\sigma_e$	1.31	S/m
axon length	$l$	10	mm
intracellular radius	$r_{in}$	0.2	mm
extracellular radius	$r_{ex}$	1	mm
myelin thickness	$t_{myel}$	0.2	mm
internodal distance	$l_{myel}$	1	mm
length of the nodes	$l_{node}$	0.1	mm
global time step	$\Delta t$	0.01	ms

Table 1: Physical and geometrical parameters.

in the conduction of action potentials in axons that are closer to the central one. Furthermore, within each axon, the nodes that are closer to the central axon also show delayed propagation, as illustrated in Figure 3. We hypothesize that this is due to the unstimulated central axon, which has an inhibitory effect on the neighboring axons, thus causing the observed delay in the transmission of action potentials.

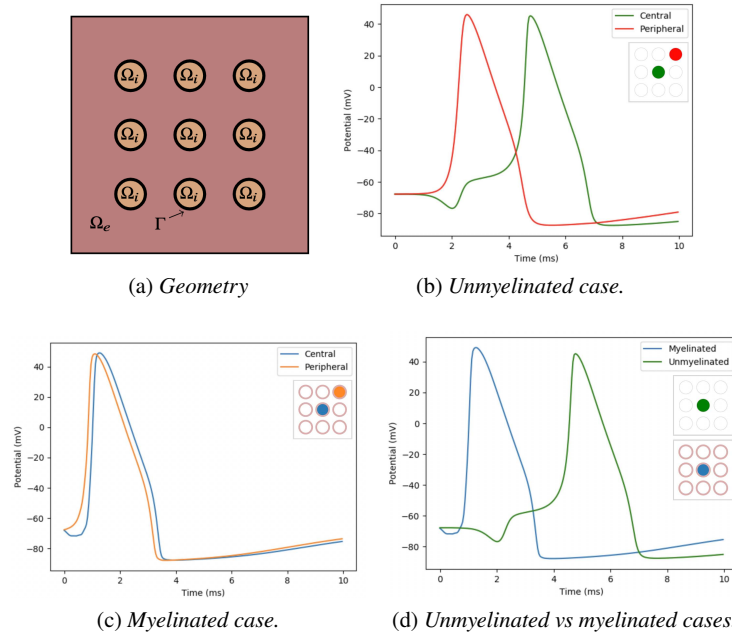


Fig. 2: Plot showing the action potentials induced in the central axon alongside (a chosen) peripheral axon in both the myelinated and unmyelinated cases.

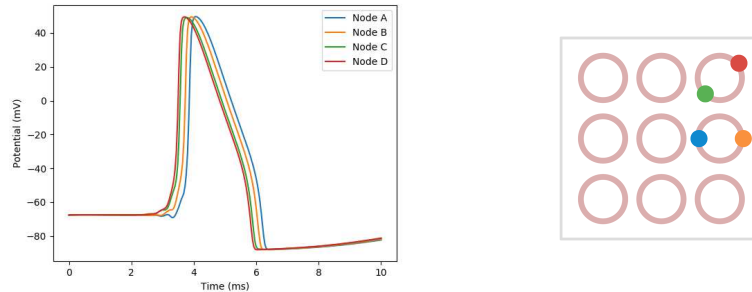


Fig. 3: Comparison of the action potential at different points (shown in the figure on the right) along the peripheral axons in the myelinated case.

## 5 Discussion

Our work is a step towards cellular scale modeling of excitable tissue with high spatial resolution, resolving realistic geometries. We analyzed how myelination affects electrical conduction in neuronal axons bundles, for the first time (to the best of our knowledge) in realistic 3D geometries. We observe increased speed in myelinated axons (as physiologically observed). Moreover, we highlight a small, but not negligible, effect of ephaptic coupling between neurons in both cases. This problem spans different scales (from  $\mu\text{m}$  to mm), coefficients jump, and requires ad hoc efficient solution strategies. An extended examination might consider the effect of varying geometrical parameters (such as the thickness of the myelin sheath), or myelin retraction. Moreover, we foresee further research using the more detailed KNP-EMI model [3, 11], an extension of the EMI model that takes into account ion concentration distribution and diffusive effects on excitable cells.

## References

1. Abdollahi, N., Prescott, S.A.: Impact of extracellular current flow on action potential propagation in myelinated axons. *Journal of Neuroscience* **44**(26) (2024)
2. Alnæs, M., Blechta, J., Hake, J., Johansson, A., Kehlet, B., Logg, A., Richardson, C., Ring, J., Rognes, M.E., Wells, G.N.: The FEniCS project version 1.5. *Archive of Numerical Software* **3**(100) (2015)
3. Benedusi, P., Ellingsrud, A.J., Herlyng, H., Rognes, M.E.: Scalable approximation and solvers for ionic electrodiffusion in cellular geometries. *SIAM Journal on Scientific Computing* **46**(5), B725–B751 (2024)
4. Benedusi, P., Ferrari, P., Causemann, M., Serra-Capizzano, S.: Dense cell-by-cell systems of PDEs: approximation, spectral analysis, and preconditioning (2024). URL <https://arxiv.org/abs/2409.13432>

5. Benedusi, P., Ferrari, P., Garoni, C., Krause, R., Serra-Capizzano, S.: Fast parallel solver for the space-time IgA-DG discretization of the diffusion equation. *Journal of Scientific Computing* **89**(1), 1–21 (2021)
6. Benedusi, P., Ferrari, P., Rognes, M.E., Serra-Capizzano, S.: Modeling excitable cells with the emi equations: spectral analysis and iterative solution strategy. *Journal of Scientific Computing* **98**(3), 58 (2024)
7. Boahen, F., Doyon, N., Deteix, J.: Sensitivity of the electrical response of a node of Ranvier model to alterations of the myelin sheath geometry. *Journal of Math. Biology* **86**(1), 17 (2023)
8. Brill, M., Waxman, S., Moore, J., Joyner, R.: Conduction velocity and spike configuration in myelinated fibres: computed dependence on internode distance. *Journal of Neurology, Neurosurgery & Psychiatry* **40**(8), 769–774 (1977)
9. Capllonch-Juan, M., Sepulveda, F.: Modelling the effects of ephaptic coupling on selectivity and response patterns during artificial stimulation of peripheral nerves. *PLOS Computational Biology* **16**(6), e1007826 (2020)
10. Dione, I., Deteix, J., Briffard, T., Chamberland, E., Doyon, N.: Improved simulation of electrodiffusion in the node of Ranvier by mesh adaptation. *PLoS one* **11**(8), e0161318 (2016)
11. Ellingsrud, A.J., Benedusi, P., Kuchta, M.: A splitting, discontinuous Galerkin solver for the cell-by-cell electroneutral Nernst–Planck framework. *SIAM Journal on Scientific Computing* **47**(2), B477–B504 (2025)
12. Fokoué, D., Bourgault, Y.: Numerical analysis of finite element methods for the cardiac extracellular-membrane-intracellular model: Steklov–Poincaré operator and spatial error estimates. *ESAIM: Mathematical Modelling and Numerical Analysis* **57**(4), 2595–2621 (2023)
13. Ford, M.C., Alexandrova, O., Cossell, L., Stange-Marten, A., Sinclair, J., Kopp-Scheinpflug, C., Pecka, M., Attwell, D., Grothe, B.: Tuning of Ranvier node and internode properties in myelinated axons to adjust action potential timing. *Nature communications* **6**(1), 8073 (2015)
14. Hodgkin, A.L., Huxley, A.F.: A quantitative description of membrane current and its application to conduction and excitation in nerve. *The Journal of physiology* **117**(4), 500 (1952)
15. Hu, Y., Schneider, T., Wang, B., Zorin, D., Panozzo, D.: Fast tetrahedral meshing in the wild. *ACM Trans. Graph.* **39**(4) (2020). DOI 10.1145/3386569.3392385
16. Huynh, N.M.M., Chegini, F., Pavarino, L.F., Weiser, M., Scacchi, S.: Convergence analysis of BDDC preconditioners for composite DG discretizations of the cardiac cell-by-cell model. *SIAM Journal on Scientific Computing* **45**(6), A2836–A2857 (2023)
17. Lopreore, C.L., Bartol, T.M., Coggan, J.S., Keller, D.X., Sosinsky, G.E., Ellisman, M.H., Sejnowski, T.J.: Computational modeling of three-dimensional electrodiffusion in biological systems: application to the node of Ranvier. *Biophysical journal* **95**(6), 2624–2635 (2008)
18. Pods, J., Schönke, J., Bastian, P.: Electrodifussion models of neurons and extracellular space using the Poisson–Nernst–Planck equations—numerical simulation of the intra-and extracellular potential for an axon model. *Biophysical journal* **105**(1), 242–254 (2013)
19. Shimba, K., Asahina, T., Sakai, K., Kotani, K., Jimbo, Y.: Recording saltatory conduction along sensory axons using a high-density microelectrode array. *Frontiers in Neuroscience* **16**, 854637 (2022)
20. Stinstra, J.G., Henriquez, C.S., MacLeod, R.S.: Comparison of microscopic and bidomain models of anisotropic conduction. In: 2009 36th Annual Computers in Cardiology Conference (CinC), pp. 657–660. IEEE (2009)
21. Tveito, A., Jæger, K.H., Lines, G.T., Paszkowski, L., Sundnes, J., Edwards, A.G., Mäki-Marttunen, T., Halnes, G., Einevoll, G.T.: An evaluation of the accuracy of classical models for computing the membrane potential and extracellular potential for neurons. *Frontiers in computational neuroscience* **11**, 27 (2017)
22. Tveito, A., Mardal, K.A., Rognes, M.E.: Modeling excitable tissue: the EMI framework. Springer (2021)
23. Xylouris, K., Queisser, G., Wittum, G.: A three-dimensional mathematical model of active signal processing in axons. *Computing and visualization in science* **13**, 409–418 (2010)
24. Xylouris, K., Wittum, G.: A three-dimensional mathematical model for the signal propagation on a neuron’s membrane. *Frontiers in Computational Neuroscience* **9** (2015)